Pergamon

Acta mater. 49 (2001) 3781–3789

Acta MATERIALIA

www.elsevier.com/locate/actamat

STUDY OF MECHANICAL DEFORMATION IN BULK METALLIC GLASS THROUGH INSTRUMENTED INDENTATION

R. VAIDYANATHAN§[1], M. DAO[1], G. RAVICHANDRAN[2] and S. SURESH[1]†

[1]Department of Materials Science and Engineering, Massachusetts Institute of Technology, Cambridge, MA 02139, USA and [2]Division of Engineering and Applied Science, California Institute of Technology, Pasadena, CA 91125, USA

(Received 14 March 2001; accepted 5 July 2001)

Abstract—Instrumented sharp indentation experiments at the nano- and micro-length scales were carried out in an attempt to quantify the deformation characteristics of Vitreloy 1™ bulk metallic glass. The experiments were accompanied by detailed three-dimensional finite element simulations of instrumented indentation to formulate an overall constitutive response. By matching the experimentally observed continuous indentation results with the finite element predictions, a general Mohr–Coulomb type constitutive description was extracted to capture the dependence of multiaxial deformation on both shear stresses and normal stresses. This constitutive response is able to provide accurate predictions of the evolution of shear bands seen in uniaxial compression tests. Constrained deformation of the material around the indenter results in incomplete circular patterns of shear bands whose location, shape and size are also captured well by the numerical simulations. The analysis is also able to predict the extent of material pile-up observed around the indenter. The surface deformation features are also consistent with mechanisms such as localized shear flow, serrated yielding and adiabatic heating, which are observed during macroscopic mechanical tests.

Keywords: Amorphous metals; Bulk metallic glasses; Indentation; Nanoindentation; Finite element method

1. INTRODUCTION

Research into the mechanical response of metallic glasses dates back to the 1960s (e.g. [1]) when it was demonstrated that thin ribbons, wires or sheets of metals in an amorphous or glass state could be produced at very high cooling rates (over 10^5 K s^{-1}). The need for the rapid cooling rate necessarily restricted the dimensions of the metallic glasses to thin cross-sections (typically less than 50 μm). A notable advance was made by Chen [2, 3] who showed that mm-scale rods of metallic glasses could be produced at cooling rates of around 10^3 K s^{-1}. In the late 1980s and 1990s, conventional foundry techniques were employed to synthesize cm-scale, "bulk" metallic glasses [4, 5]. Since these metallic glasses could be produced in bulk form, the mechanical properties of the amorphous alloys became topics of considerable research for possible structural applications. Of these alloys, Zr-based bulk metallic glasses have been commercially developed into engineering materials (e.g. as Vitreloy 1™ [6]). Given their potential use as engineering materials, there is a concomitant need to establish their mechanical properties. Although there is growing interest in the mechanical properties of bulk metallic glasses, systematic experiments and analysis of their constitutive behavior under general multiaxial loading conditions have thus far not been conducted.

The deformation of polycrystalline metals and alloys are generally characterized by recourse to the von Mises continuum plasticity theory with isotropic or kinematic hardening laws and the normality flow rule (e.g. [7]). The mechanisms of microscopic plastic deformation in crystalline alloys are strongly influenced by the local shear stresses, without any pronounced effects on deformation from the local tensile or hydrostatic stresses (in the absence of such ductile failure processes as void nucleation and growth). The mechanical deformation characteristics of metallic glasses, however, differ in many respects. First, amorphous metals do not exhibit any strain hardening. Second, available experiments also strongly suggest that their elastoplastic deformation response is influenced by the shear as well as the normal compo-

† To whom all correspondence should be addressed. Tel.: +1-617-253-3320; Fax: +1-617-253-0868.
E-mail address: ssuresh@mit.edu (S. Suresh)
§ Current address: Advanced Materials Processing and Analysis Center and Mechanical, Materials and Aerospace Engineering, University of Central Florida, Orlando, FL 32816, USA

1359-6454/01/$20.00
PII: S1359-6454(01)00263-4

nent of the local stress, and possibly by the hydrostatic stress [8, 9]. Third, the deformation of metallic glasses occurs highly inhomogeneously through the concentration of inelastic strains in localized shear bands. In unconstrained geometries, such as an uniaxial tensile test, a dominant shear band could traverse the entire cross section of the specimen, while multiple shear bands develop in constrained geometries, such as an uniaxial compressive test, giving rise to large-scale inelastic deformation and an overall elastic-perfectly-plastic deformation response.

In order to elucidate the multiaxial deformation characteristics of bulk metallic glasses, systematic, multiaxial experiments involving different combinations of normal and shear loading are inevitably required. The paucity of such information, however, is mainly due to the lack of availability of sufficient quantities of the metallic glasses to perform "valid" mechanical tests on specimens of sufficiently large dimensions, and due to the costs and time associated with performing such tests. These difficulties could be circumvented, at least in part, by conducting instrumented indentation tests at multiple length scales whereby a variety of multiaxial deformation characteristics of the metallic glasses could be assessed in a systematic manner. Continuous, depth-sensing, multi-scale indentation, which provides a record of the indentation load as a function of the indenter penetration depth into the material during the application and removal of the load, affords the flexibility to examine small specimen volumes (see e.g. [10–13]). Furthermore, the plastic deformation region around the indenter is constrained by the surrounding elastic material, thereby suppressing the unstable extension of dominant shear bands. The overall load–displacement curves obtained during instrumented indentation provide valuable information about the macroscopic deformation characteristics of the metallic glasses, whereas the locations, dimensions and shapes of the shear bands as well as the extent of material pile-up around the indenter provide useful insights into the microscopic deformation characteristics of the material. Multi-scale, instrumented indentation can thus serve as a global and local probe into the constitutive response of metallic glasses.

The objective of this work was to conduct a combined experimental and computational study of multi-scale indentation of a Zr-based bulk metallic glass in order to extract quantitative information about its inelastic deformation characteristics. Experimental studies of nano- and micro-scale sharp indentation, in conjunction with full three-dimensional finite element computations, are used to determine the yield criterion as well as the conditions for the formation of shear bands.

2. MATERIAL AND EXPERIMENTAL METHODS

The material investigated in this study is an as-cast, fully amorphous, $Zr_{41.25}Ti_{13.75}Cu_{12.5}Ni_{10}Be_{22.5}$ (nominal composition in at.%) alloy, manufactured by Howmet Corporation, Greenwich, CT (trade name Vitreloy 1). Sharp indentation experiments were performed in a Nanoinstruments Nanoindenter II™ (Nanoinstruments, Inc. Tennessee, USA). Given the need to obtain accurate data for quantitative evaluation, the results obtained with the Nanoindenter II™ were also compared and contrasted with those measured with a NanoTest 600™ nano/micro-indenter from Micro Materials Limited, Wrexham, UK. Additionally, a combination of multiple indents (at least four) on multiple specimens (at least two) was used to verify the accuracy and scatter of the indentation data. A diamond Berkovich indenter, nominally sharp but with a finite tip radius of 40–50 nm, was used in experiments conducted with a maximum load of 10 N. For the low-load indents (below 10 mN), a Dynamic Contact Module™ (DCM) was placed in series with the load train to obtain better load and depth resolution [14]. The loading and unloading phases of indentation were carried out under load control (nominal rate of 0.01 mN s^{-1}). At maximum load, a dwell period of 20 s was imposed before unloading, and another dwell period of 20 s at 90% of unloading, so as to correct for any thermal drift in the system. The specimen dimensions were $2\times0.7\times0.3$ cm and adjacent indents were separated by at least 10 μm. The indents were examined using a Tencor P-10™ Profiler (KLA-Tencor, San Jose, CA) and a scanning electron microscope (SEM).

3. COMPUTATIONAL MODELING

A three-dimensional finite element (FE) model incorporating the inherent six-fold symmetry of a Berkovich indenter was constructed to simulate the indentation of metallic glass. A total of 11,040 eight-noded, isoparametric elements were used to capture deformation modes. Figure 1(a) shows the overall mesh design, while Fig. 1(b) details the area that directly contacts the indenter tip. Computations were performed using the general purpose finite element package ABAQUS [15], assuming finite deformation characteristics (i.e., maximum total strains under the indenter typically well in excess of 5%). The mesh design was authenticated with results from the mesh used previously by Larsson *et al*. [16].

In this study two elastoplastic constitutive laws were used, namely a von Mises continuum plasticity model and a Mohr–Coulomb model. The von Mises yield criterion, where the deformation is assumed to be independent of pressure, is written as:

$$(\sigma_1-\sigma_2)^2 + (\sigma_2-\sigma_3)^2 + (\sigma_3-\sigma_1)^2 = 6k^2 = 2\sigma_y^2, \quad (1)$$

where σ_1, σ_2, σ_3 are the principal stresses and $k = \sigma_y/\sqrt{3}$, where σ_y is the yield strength measured in a uniaxial tension test. Some prior experimental stud-

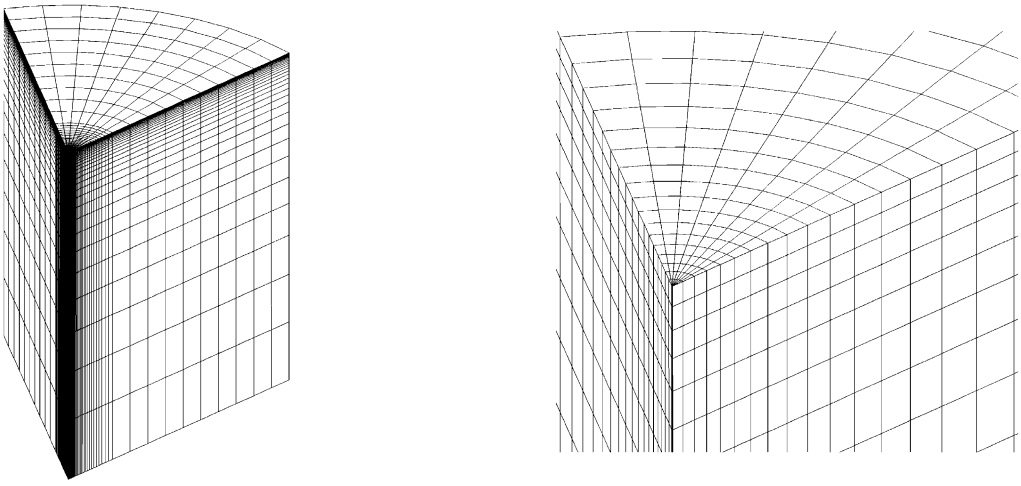

Fig. 1. (a) Overall mesh design used in the finite element simulations. (b) Detailed view of area in direct contact with the indenter tip.

ies (e.g. [17, 18]) have postulated that the von Mises yield criterion adequately models the deformation characteristics of bulk metallic glasses. Alternatively, the Mohr–Coulomb criterion, where the plastic flow is assumed to be influenced by the local normal stress, is generally written for metallic glasses as [8, 9]

$$\tau_c = k_0 - \alpha\sigma_n \tag{2}$$

where τ_c is the shear stress on the slip plane at yielding, k_0 and α are constants and σ_n is the stress component in the direction normal to the slip plane.

In the present three-dimensional computational simulations of indentation, both the von Mises and Mohr–Coulomb plastic yield criteria were invoked in the material model in order to predict the indentation load–displacement response as well as the stress and deformation fields around the indentation contact region. By matching such predictions with experimental measurements of load versus displacement and of the shear band characteristics, the material parameters in the above yield criteria were extracted from the numerical models. For both yield models, the material was assumed to possess isotropic properties, and appropriate flow potentials were assumed. The detailed integration schemes of the constitutive models can be found in [15]. The maximum total strain under a sharp Berkovich indenter was expected to exceed 10–20% and was confirmed in the computations. In all the numerical results presented in this paper, a finite deformation analysis was consequently employed. When the normal stress dependence coefficient, α, [see equation (2)] is not zero, plastic flow in the Mohr–Coulomb model is non-associated. Therefore the exact tangent stiffness matrix is not symmetric. In order to ensure the proper and efficient convergence of the computations in this case, a non-symmetric tangent stiffness matrix was used at each iteration.

4. EXPERIMENTAL RESULTS AND ANALYSES

Figure 2 shows the variation of indentation load as a function of indenter penetration depth into the metallic glass (during loading) from two series of indentation experiments (to depths of 35 and 50 nm). The nanoindentation results shown in Fig. 2 ensure sufficiently small loads where only elastic deformation is induced in the metallic glass. For a Berkovich indenter, the relationship between load, P, and indentation depth, h, has been established [16, 19] through the elastic indentation stiffness, C, as:

$$P = Ch^2 = 2.1891(1 - 0.21\nu_i - 0.01\nu_i^2 - 0.41\nu_i^3)E^* h^2 \tag{3}$$

where ν_i is Poisson's ratio of the indented material

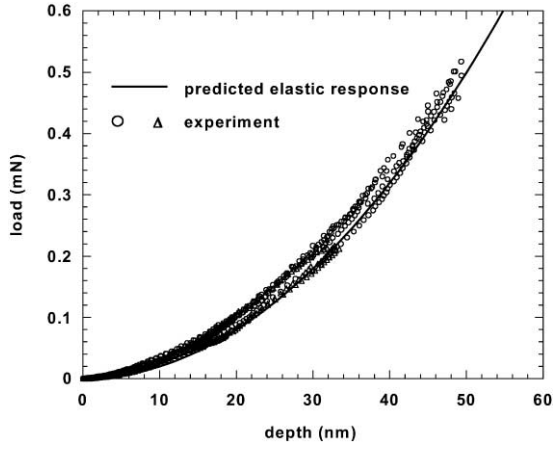

Fig. 2. Nanoindentation response of metallic glass during elastic loading. Two series of experiments (distinguished by different symbols) to depths of 35 and 50 nm, consisting of four and six individual indents, respectively, are shown. The triangles correspond to a maximum depth of indentation of 35 nm and the circles correspond to a maximum depth of 50 nm.

and E^* is an effective modulus. This effective modulus includes the elastic moduli of the specimen and the indenter, (E_s and E_i, respectively) and the corresponding values of Poisson's ratio (ν_s and ν_i, respectively):

$$E^* = \left[\frac{1-\nu_i^2}{E_i} + \frac{1-\nu_s^2}{E_s}\right]^{-1} \quad (4)$$

Using values of $E_i = 1000$ GPa and $\nu_i = 0.07$ for the diamond indenter, and $E_s = 96$ GPa and $\nu_s = 0.36$ for the metallic glass [20], a value of 100 GPa was obtained for the effective modulus from equation (4). The corresponding predicted value for the elastic indentation stiffness is 200 GPa from equation (3). This predicted response is shown in Fig. 2 and is in agreement with the loading portion of the two series of indentation experiments.

Figure 3 shows the results of nanoindentation experiments where the metallic glass was indented to depths of 5 and 9 μm in two sets of indentation tests. The unloading portion of the load–depth response is also shown in Fig. 3 and the loading condition in this figure is such that appreciable inelastic deformation occurs. Figures 2 and 3 clearly illustrate the reproducibility of nano- and micro-indentation data obtained from multiple tests in this work.

Using known [20] elastic properties and yield strength data for the metallic glass used in the present indentation tests (i.e., elastic modulus of 96 GPa, Poisson's ratio of 0.36 and tensile yield strength of 1.9 GPa), finite element simulations were carried out, employing the methods described in Section 3, to generate predictions of indentation load versus penetration depth curves assuming either the von Mises or the Mohr–Coulomb yield criteria. For the latter, the constants were established so as to satisfy macroscopic tensile yielding at 1.9 GPa while varying the value of α [see equation (2)]. Numerical predictions of the complete indentation load–displacement curves (loading and unloading portions) for the elastic deformation as well as the elastoplastic deformation, extracted by assuming either the Mises or Mohr–Coulomb criteria, are superimposed on the experimental data in Fig. 3. From Fig. 3, it appears that the metallic glass does not follow the von Mises criterion. The load–depth prediction using a Mohr–Coulomb criterion (with $\alpha = 0.13$) follows the experimental results more closely, suggesting the influence of a normal stress component on yielding. This value of $\alpha = 0.13$ used in the FE simulation compares well with the value of 0.11±0.05 previously reported by Donovan [8] for $Pd_{40}Ni_{40}P_{20}$ metallic glass.

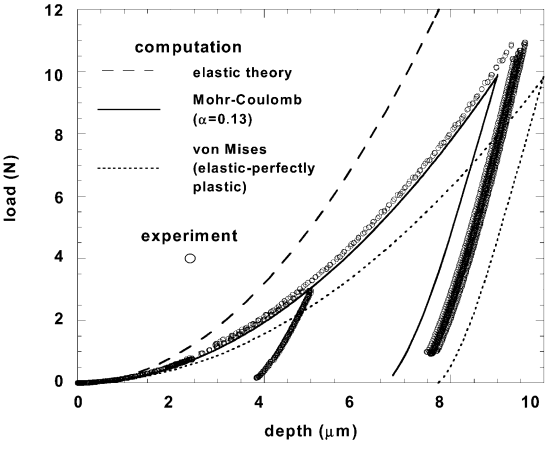

Fig. 3. Microindentation response of metallic glass during loading and unloading. Two series of experiments to depths of 5 and 9 μm, consisting of five and eight individual indents, respectively, are shown.

Figure 4(a) is a representative optical micrograph showing an impression from a 9 μm deep indentation. The characteristic circular patterns around such indents constitute "pile-up" and an SEM image showing the inherent topology is shown in Fig. 4(b). The surface uplift of the pile-up, characterized using a profilometer, is shown in Fig. 4(c). The representative indent in Fig. 4(a) is surrounded by characteristic circular patterns. The SEM image in Fig. 4(b) and the profilometry results in Fig. 4(c) clarify that the features around the indent are not cracks but represent overlapping layers of displaced material as a result of the indenter. For non-strain hardening materials, the plastically displaced material is expected to flow up to (and "pile-up" against) the faces of the indenter due to the incompressibility of plastic deformation. This is particularly true in the case of metallic glasses given their tendency to deform in an elastic-perfectly-plastic manner. Hence, the pile-up observed around indents is consistent with the macroscopic stress–strain response. The corresponding deformation features on the impression from the indenter face are shown in Fig. 5. This SEM image was obtained by tilting the sample so as to facilitate such an observation. Concentric shear bands on an impression from the indenter face are seen in this micrograph. Figures 6(a) and (b) are SEM images that further examine the structure of the shear bands generated by indentation. These bands are a result of the tendency of metallic glasses to deform in a highly localized manner, even at these scales. Figures 6(a) and (b) show representative wavy, flowing patterns in the pile-up that are indicative of viscous flow. Elevations in temperature due to adiabatic heating can aid in the formation of such patterns. Thermodynamic calculations based on the conversion of stored elastic strain energy to adiabatic heating of the shear band region estimate highly localized surges in temperatures exceeding the melting point during macroscopic tension tests [21].

5. DISCUSSION

The dependence of yield strength on the normal stress acting on the slip plane necessitates that the slip plane deviate from the plane of maximum resolved

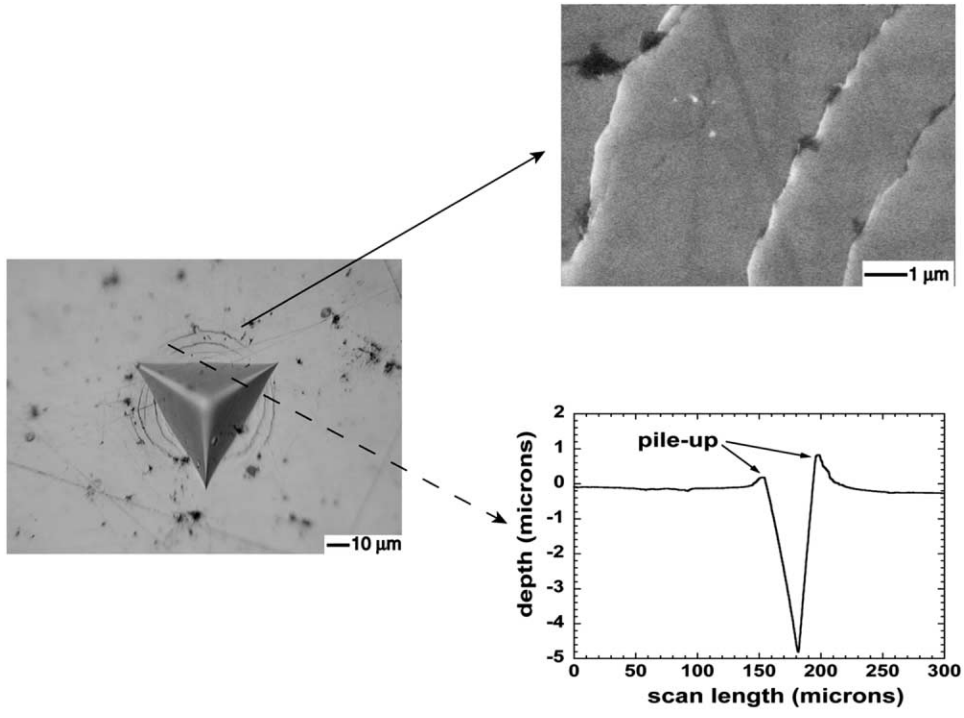

Fig. 4. (a) Optical micrograph of a 9 μm deep Berkovich indent. (b) Overlapping bands in pile-up around indent. (c) Asymmetric trace across indent using a profiler.

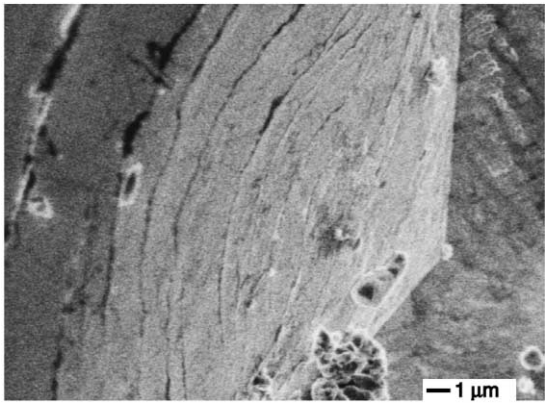

Fig. 5. Shear bands on impression from Berkovich indenter face.

shear stress in equation (2) [22]. Taking the effective loading stress as

$$\tau_{\text{eff}} = \tau_{\text{c}} + \alpha\sigma_{\text{n}}, \tag{5}$$

the Mohr–Coulomb yield criterion [equation (2)] can be expressed as

$$\tau_{\text{eff}} = k_0. \tag{6}$$

When the specimen is subject to a uniaxial compressive stress $-\sigma$ ($\sigma>0$), equation (6) can be rewritten as

$$\tau_{\text{eff}} = \sigma\sin\theta\cos\theta - \alpha\sigma\sin^2\theta = k_0, \tag{7}$$

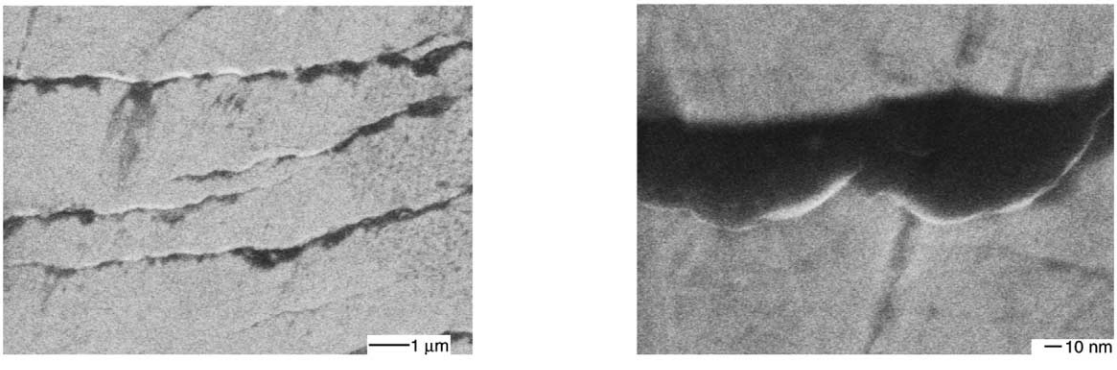

Fig. 6. (a) and (b) Structure of shear bands showing wavy and flowing patterns.

where θ is the angle between the slip plane and the loading axis. Taking the derivative of τ_{eff} with respect to θ gives

$$\frac{\partial \tau_{\text{eff}}}{\partial \theta} = \sigma(\cos 2\theta - \alpha \sin 2\theta). \tag{8}$$

The minimum effective loading stress, τ_{eff}, is obtained when

$$\frac{\partial \tau_{\text{eff}}}{\partial \theta} = \sigma(\cos 2\theta - \alpha \sin 2\theta) = 0. \tag{9}$$

If $\alpha = 0$, solving equation (9) gives $\theta = 45°$; if $\alpha = 0.13$, $\theta = 41.3°$ is predicted. Due to the absence of strain hardening, the specimen is expected to experience strain localization immediately after the initial yielding along the slip plane [23]. Recently microscopic observations of a compression test specimen were made in an $Zr_{41.25}Ti_{13.75}Cu_{12.5}Ni_{10}Be_{22.5}$ alloy after its failure [24]. The experimentally observed angle ($\approx$42°) between the shear bands and the loading axis appears to agree with this value of 41.3°. Here we note that the inclination of the bands at the instant they form may differ from the inclination measured after unloading because of the large elastic recovery on unloading. Nevertheless, the value of α, used to formulate an overall constitutive response to describe the multiaxial deformation of metallic glass under an indenter, appears to correctly predict the evolution of shear bands in a uniaxial test.

Free volume or dilatation models [25, 26] proposed to describe deformation in such glasses involve the accumulation of free volume during localized shearing. Consequently, such deformation mechanisms would be expected to be pressure sensitive and depend on the hydrostatic component of the applied stress. Thus, we expect the observed normal stress dependency to arise from such a pressure dependency. However, direct measurements have so far indicated that the pressure dependency of the yield strength of a metallic glass is small [8, 9]. While we conclusively establish that the yielding cannot be described by a von Mises criterion and involves a normal stress component, we cannot conclude whether the normal stress dependence is distinct from any pressure dependency that may exist. The reason for this uncertainty arises due to the possibility of changing the predicted load–depth response by

1. modifying the value of α, or
2. by incorporating an additional pressure sensitive term i.e., a term proportional to $(\sigma_1 + \sigma_2 + \sigma_3)/3$ in equation (2).

This is quantitatively illustrated in Fig. 7 wherein two load–depth responses, from FE simulations with $\alpha = 0.10$ and 0.13, are shown and the difference could be corrected by a combination of normal and/or pressure sensitive terms in the yield criterion. It is clear that the effect of these normal stress or pressure dependent terms in the yield criterion on common deformation modes is small.

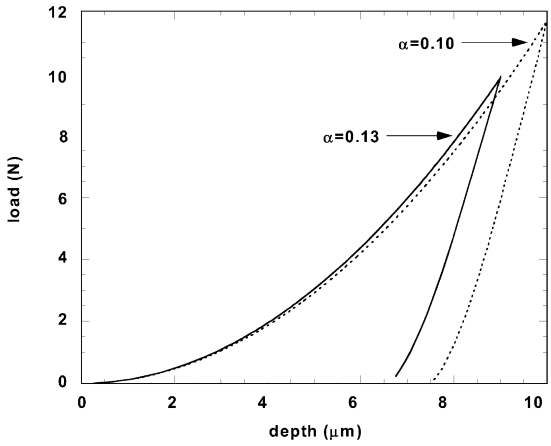

Fig. 7. Load depth response as predicted from finite element simulations using a Mohr–Coulomb criterion with $\alpha = 0.13$ and 0.10.

The computational simulations were also used to assess the extent of pile-up around the indenter. An experimentally observed profile is compared with computational results in Fig. 8. Despite using macroscopic stress–strain data and a continuum-based approach, we note that the simulation captures the experimentally observed pile-up reasonably well. The circular patterns that constitute pile-up are distinct in that they are incomplete. Again, the finite-element simulations were used to examine the stress fields around the imprint of the indenter in order to examine this distinctive feature. Figure 9(a) shows the contours (in plan view) of the normalized Mises equivalent stress on the surface of the specimen after unloading the indenter (following a 9 μm indentation experiment). Figure 9(b) is the corresponding figure

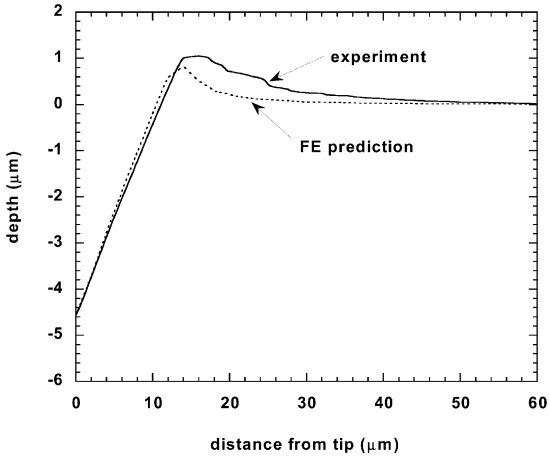

Fig. 8. Experimental profile of pile-up compared with finite element simulation.

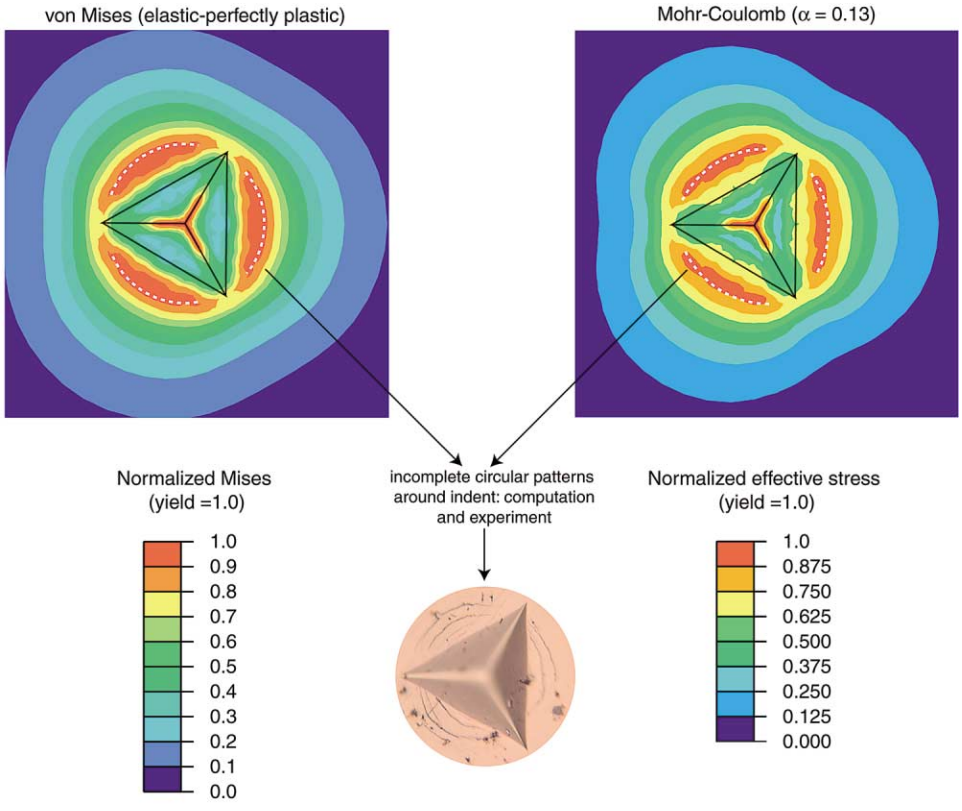

Fig. 9. Plan view of contours corresponding to (a) the Mises equivalent stress and (b) the Mohr–Coulomb effective stress [equation (5)] on the surface of the specimen upon unloading after a 9 μm deep indentation experiment. The position of the indenter along with (c) a micrograph scaled to the size of the simulation is also shown.

showing the normalized effective stress [equation (5)]. The position of the indenter is also shown, along with an optical micrograph [Fig. 9(c)] scaled to correspond to the size of the simulation. The residual stress fields do indeed predict a circular plastic zone around the imprint and importantly, this zone is not complete as seen in the form of lower stresses at the indenter corners. The dashed lines in the computational predictions correspond to the locations of the local maximum effective stresses at which the shear bands would be expected to nucleate. Note the good agreement between the predicted shapes, sizes and locations of shear bands around the indents and those observed experimentally. It should also be noted here that the above simulations of the pile-up do not depend on the choice of either the von Mises or the Mohr–Coulomb yield criterion, suggesting again that the normal stress dependence is not sufficiently large to affect the local shear band characteristics around the indents.

However, a continuum FE approach cannot predict multiple, overlapping concentric rings in the pile-up, which are expected to be discrete in their origin. The existence of these multiple rings is consistent with serrated plastic flow observed during macroscopic tests [27, 28]. Such yield drops are expected to correspond to the formation of new shear bands. It is therefore possible that the generation of new shear bands and/or secondary shear bands from primary shear bands result in the observed overlapping concentric rings. On examining and simulating the observed features following indentation, it can be summarized that they are consistent with mechanisms observed in macroscopic tests and arise due to a combination of discrete and continuum phenomena.

Metals (both in single crystalline and polycrystalline form) exhibit periodic displacement bursts associated with the nucleation and propagation of dislocations at essentially constant loads during load-controlled indentation [13, 29]. The first displacement burst appears to occur when the maximum shear stress at the indenter tip is of the order of the theoretical shear strength of the material. The punching of arrays of dislocation within the grains surrounding the indentation has also been directly observed in transmission electron microscopy studies of indented polycrystalline Cu films [13, 30]. For the case of the metallic glass and the chosen indenter no such displacement bursts were observed, despite the onset of deviation from the predicted elastic response. Here we note that we distinguish between the existence of characteristically consistent displacement bursts (such as those previously observed in polycrystalline metals) and displacement discontinuities or “pop-ins”

(such as those previously observed in Ref. [31]). This suggests that plasticity events in metallic glasses, when constrained by surrounding undeformed material and subject to multi-axial loading (as in during indentation), can occur at length scales below the resolution of existing instrumentation (0.5 nm) and can be contrasted with bursts during indentation of crystalline metals that typically involve displacements between 5 and 15 nm using a similar indenter [13].

The obvious lack of dislocation nucleation and propagation in metallic glass is expected given the lack of any long-range order in these materials. However, it is interesting to observe this reduced length scale associated with the initiation of plasticity in metallic glasses. This can be directly contrasted with macroscopic tests of metallic glasses where a single shear band propagating catastrophically in a tensile test specimen fails with almost no plastic strain. An equivalent compressive test specimen can exhibit plastic strains of over 2.5% (above the 2% elastic strains) due to the formation of multiple shear bands [17] that are constrained by the applied compressive stress. Thus, while instabilities occur as displacement bursts during the small scale deformation of crystalline metals under an indenter, large scale deformation usually involve the suppression of these instabilities resulting in plasticity. On the contrary, while no displacement bursts are observed in metallic glass during small scale indentation tests, macroscopic tests (in the absence of geometrical constraints) usually involve limited plastic deformation due to unstable shear band propagation. This points to the existence of a strain energy accommodation mechanism in metallic glass that chooses between nucleation and propagation of shear bands and consequently results in multiple shear bands or a few dominating shear bands. It is therefore reasonable to expect that varying the indenter tip size/geometry may favor a few dominating shear bands and result in the observation of displacement bursts.

Constrained deformation underneath the indenter can also result in local crystallization in regions of high inelastic deformation, which in turn can lead to local density changes. Electron diffraction patterns in regions immediately beneath the indentation in the amorphous metal appear to validate such a hypothesis [32]. Furthermore, local adiabatic heating due to constrained deformation can assist the crystallization of the metallic glass.

6. CONCLUSIONS

By recourse to instrumented indentation of $Zr_{41.25}Ti_{13.75}Cu_{12.5}Ni_{10}Be_{22.5}$ bulk metallic glass over nano- and micro-scales, the following conclusions are made:

1. The predicted elastic load–depth response is in close agreement with experiments.
2. On comparing the load–depth relationship corresponding to elastoplastic deformation with FE simulations, it is established that the material does not follow the von Mises criterion as previously suggested [17, 18]. The observed experimental results are consistent with FE simulations using a Mohr–Coulomb yield criterion, suggesting the influence of a normal stress component.
3. For the indenter used, the transition from elastic to elastoplastic behavior is mostly gradual (within the resolution of existing instrumentation) and is characteristically devoid of consistent displacement bursts, such as those previously observed in polycrystalline metals. On comparing this gradual transition from elastic to elastoplastic behavior with the phenomenon of catastrophic shear band propagation in macroscopic tests, it is expected that varying the indenter tip size/geometry may favor a few dominating shear bands and result in the observation of displacement bursts.
4. A continuum FE based approach successfully simulated distinctive, incomplete circular patterns in the pile-up that exists around an indent following unloading.

Acknowledgements—The authors are grateful to T.-G. Nieh, B.W. Choi, K.J. Van Vliet, J. Smith and A. Gouldstone for valuable experimental assistance, and to W.L. Johnson and J. Lu for providing the specimens. Useful discussions with F. Spaepen are also gratefully acknowledged. GR would like to thank the Army Research Office and the NSF MRSEC program for the support of his research in bulk metallic glasses (BMG).

REFERENCES

1. Clement, W., Willens, R. H. and Duwez, P., *Nature*, 1960, **187**, 869.
2. Chen, H. S., *Acta metall.*, 1974, **22**, 1505.
3. Chen, H. S., *Rep. Prog. Phys.*, 1980, **43**, 353.
4. Inoue, A., *Acta mater.*, 2000, **48**, 279.
5. Johnson, W. L., *MRS Bull.*, 1999, **24**(10), 42.
6. Manufactured by Howmet Corporation, Greenwich, CT and marketed by Liquid Metal Golf Inc., Laguna Miguel, CA.
7. Hill, R., *Mathematical Theory of Plasticity*. Oxford University Press, Oxford, 1998.
8. Donovan, P. E., *Acta metall.*, 1989, **37**, 445.
9. Lowhaphandu, P., Montgomery, S. L. and Lewandowski, J. J., *Scripta mater.*, 1999, **41**, 19.
10. Giannakopoulos, A. E. and Suresh, S., *Scripta mater.*, 1999, **40**, 1191.
11. Venkatesh, T. A., Van Vliet, K. J., Giannakopoulos, A. E. and Suresh S., *Scripta mater*. 2000, **41**, 14.
12. Suresh, S. and Giannakopoulos, A. E., *Acta mater.*, 1998, **46**, 5755.
13. Gouldstone, A., Koh, H. -J., Zeng, K. -Y., Giannakopoulos, A. E. and Suresh, S., *Acta mater.*, 2000, **48**, 2277.
14. Lucas, B. N., Oliver, W. C. and Swindman, J. E., in *Materials Research Society Symposium Proceedings*, Vol. 522, ed. N. R. Moody, W. W. Gerberich and S. P. Baker. Materials Research Society, Warrendale, PA, 1998, p. 3.
15. *ABAQUS, General Purpose Finite Element Program, Version 5.4*. Hibbit, Karlsson and Sorensen Inc, Pawtucket, RI, 1995.
16. Larsson, P. - L, Giannakopoulos, A. E., Soderlund, E., Rowcliffe, D. J. and Vestergaard, R., *Int. J. Solids Struct.*, 1996, **33**, 221.

17. Bruck, H. A., Christman, T., Rosakis, A. J. and Johnson, W. L., *Scripta metall.*, 1994, **30**, 429.
18. Kimura, H. and Matsumoto, T., in *Amorphous Metallic Alloys*, ed. F. E. Luborsky. Butterworth and Co Ltd, London, 1983, p. 187.
19. Suresh, S., Alcala, J. and Giannakopoulos, A. E., US Patent No. 6,134,954, 2000.
20. Conner, R. D., Dandliker, R. B. and Johnson, W. L., *Acta mater.*, 1998, **46**, 6089.
21. Liu, C. T., Heatherly, D. S., Easton, D. S., Carmichael, C. A., Schneibel, J. H., Chen, C. H. et al., *Acta metall. mater. Trans.*,, 1998, **29A**, 1811.
22. Bowden, P. B. and Jukes, J. A., *J. Mater. Sci.*, 1972, **7**, 52.
23. Asaro, R. J. and Rice, J. R., *J. Mech. Phys. Solids*, 1977, **25**, 309.
24. Wright, W. and Nix, W. D., Stanford University, CA, private communication, 2001.
25. Spaepen, F., *Acta metall.*, 1977, **25**, 407.
26. Argon, A. S., *Acta metall.*, 1979, **27**, 47.
27. Hufnagel, T. C., El-Deiry, P. and Vinci, R. P., *Scripta metall.*, 2000, **43**, 1071.
28. Pampillo, C. A., *J. Mater. Sci.*, 1975, **10**, 1194.
29. Corcoran, S. G., Colton, R. J., Lilleodden, E. T. and Gerberich, W. W., *Phys. Rev. B*, 1997, **55**, 16057.
30. Gerberich, W. W., Nelson, J. C., Lilleodden, E. T., Anderson, P. and Wyrobek, J. T., *Acta mater.*, 1999, **9**, 3585.
31. Wang, J. G., Choi, B. W., Nieh, T. -G. and Liu, C. T., *J. Mater. Res.*, 2000, **15**, 798.
32. Kim, J.-J., Vaidyanathan, R., Choi, Y.-J and Suresh, S., unpublished research, Massachusetts Institute of Technology, Cambridge, 2001.